Superheater Design Assessment for Flexible Solar Tower Plants

T. Rodríguez-Reviejo[1], P.A. González-Gómez[1], M. Laporte-Azcué[1], D. Santana[1]

[1]Energy Systems Engineering Group (ISE), Department of Thermal and Fluid Engineering, University Carlos III of Madrid, Leganés (Spain).

Abstract

The steam generator failure is one of the main causes of unavailability of commercial solar tower plants. The superheater, as the point most susceptible to failure due to creep-fatigue damage, should be carefully analyzed to assure suitable reliability levels. For that reason, in this work, a novel superheater based on the header-type design is selected for a structural comparison study against to the conventional design consisting in a shell-and-tube hairpin-type superheater.

Keywords: Steam generator, Creep-fatigue, Lifetime, Transient operation

1. Introduction

Solar tower plants have become a renewable solution able to play the role of load following plants like combined cycles (Mehos et al., 2017), which have a key role in modern electricity markets with high penetration of variable renewable energies. In this context, solar power plants are pushed to operate with fast start-ups and/or load changes to meet users demand and counter-balance grid stability issues. However, aggressive operations lead to an increase of the fatigue damage which may be combined with creep, leading to an extraordinary lifetime reduction on critical components like superheaters. Therefore, the correct selection of the superheater design has become a critical step to achieve the required levels of reliability and flexibility of solar tower plants.

The superheater, as a critical point of the steam generator system (SGS), has a high influence on the performance and forced outages of the plant. According to the Concentrating Solar Power Best Practices Study (Mehos et al., 2020), the system with the highest number of issues occurred in commercial solar tower plants was related to the steam generator reliability and design. Figure 1 shows the main issues reported plotted by priority and number of occurrences. As it can be noticed, the ones that appear at the upper-right quadrant are the main issues for the industry. This also has further effects in costs and maintenance, which appear to be greater than predicted in previous studies. Numerous problems related to reliability and availability have occurred due to the conventional steam generator design based on shell-and-tubes with flat tube sheets. For that reason, a novel model of heat exchanger called Header-type is going to be analyzed.

In the open literature can be found some works focused on the structural integrity assessment of steam generators for concentrating solar power plants (Ferruzza et al., 2019; González-Gómez et al., 2019, 2018). In the case of parabolic trough plants, the main mechanism of damage is fatigue due to the low working temperatures and the used standards were the EN-12952-3 and the ASME Section VIII-Div2. The high working temperatures of solar tower plants lead to a significant creep damage which may be combined with fatigue, and at such conditions the recommended code is ASME III-Subsection NH.

2. Case of study

A conventional molten-salt solar tower plant of 110 MWe Rankine cycle has been selected for the analysis. The main plant layout can be studied in Figure 2, where the main focus should be the steam generator. The steam generator consists of an indirect steam generator system where the hot fluid is molten salt (i.e., 60% NaNO3 and 40% KNO3) which is heated at the receiver (R) using solar radiation and then enters the steam generator system when it is required. It is stored in both cold and hot tanks (CT, HT). The cold fluid is water/steam which flows through the SGS in order to produce steam and expand at the power block. The steam generator is formed by four heat exchangers: superheater (SH), reheater (RH), evaporator (EV) and preheater (PH). Water/steam and salt properties are calculated according to (Wagner and Kretzschmar, 2008) and (NREL, 2009) respectively.

doi:10.18086/swc.2021.13.01 Available at http://proceedings.ises.org

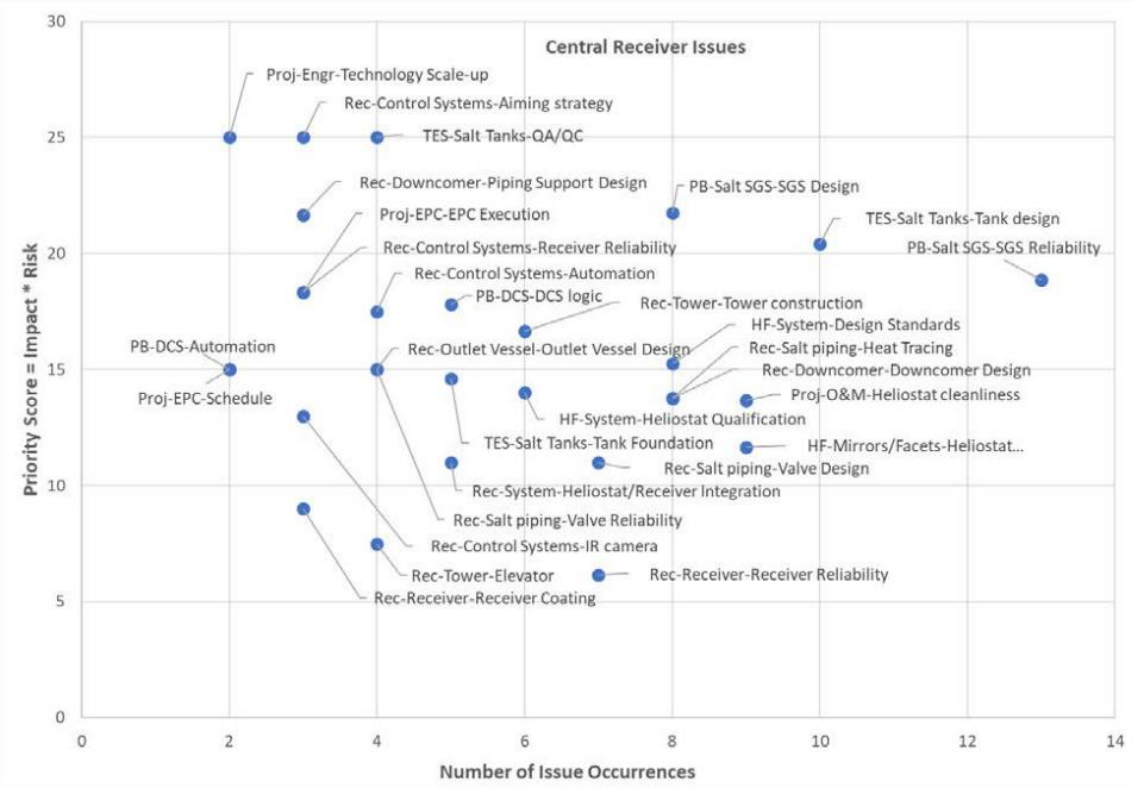

Fig. 1: Main issues reported at central receiver CSP plants plotted by priority and number of occurrences (Mehos et al., 2020)

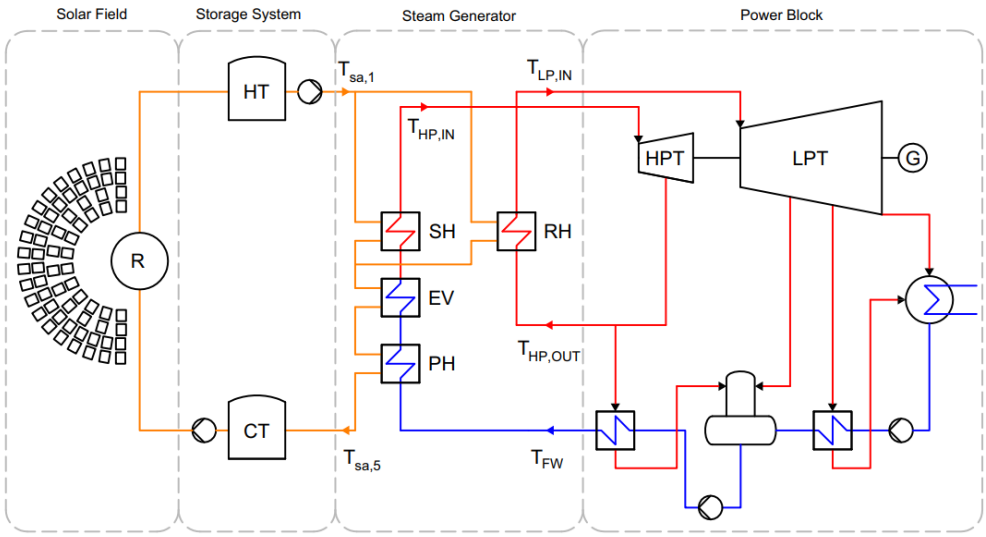

Fig 2. Plant layout.

Besides the commonly-used Hairpin-type, a novel model of heat exchanger called Header-type is going to be studied as well. The working system and its geometry can be seen in Figure 3. The water or steam enters the heat exchanger through the inlet header, flows through the different coils and goes out across the outlet header. This process happens in multiple layers. On the other hand, the salt flows on the shell side between the tube bundle. Header-type superheater is going to be analysed against the Hairpin-type to confirm its excellent performance shown in different studies (Mehos et al., 2020) as there is no highly reliable data about this topic. Its manufacturer, Aalborg CSP (Aalborg CSP, 2021) reported no leakage in commercial service. In order to obtain the design and main specifications of the SGS, 4 individual optimizations are carried out. The geometry obtained for both hairpin-

type and header-type are presented in Table 1.

From creep-fatigue point of view the most critical component is the superheater. This is because the superheater has to withstand the highest temperatures, which are combined with high temperature gradients which induce large stress variations and fatigue, and all of this may lead to a premature creep-fatigue failure. In Figure 3 the potential critical points of the superheater designs selected for this study are shown.

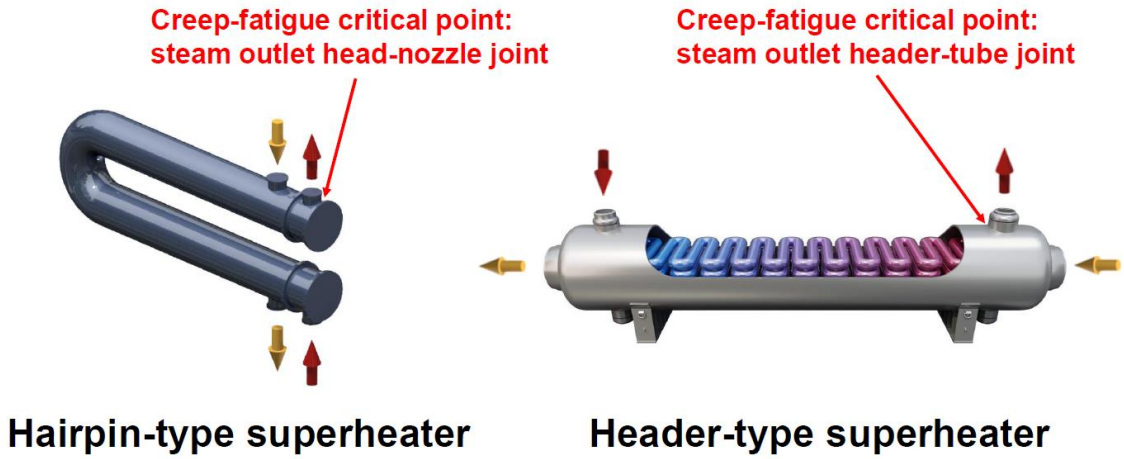

Fig. 3: Selected superheater designs and critical points. Right: hairpin-type; Left: header-type (Aalborg CSP, 2021).

Tab. 1. Geometry of both hairpin-type and header-type superheaters.

	Hairpin-type	Header-type
Head/header outer diameter (mm)	842	466
Head/header thickness (mm)	130	66.2
Nozzle/tube outer diameter (mm)	404	25
Nozzle/tube thickness (mm)	77	3.1

Once the design of the SH is known, the thermo-mechanical analysis is implemented. The operation of the steam generator selected for the study is the warm startup (González-Gómez et al., 2019). The initial temperature of the heat exchanger is 290ºC which is the set point to prevent the salt from freezing. The initial pressure matches the saturation pressure at 290ºC, i.e. 74 bar. The main trends of the temperature and pressure for the superheater are illustrated in Figure 4.

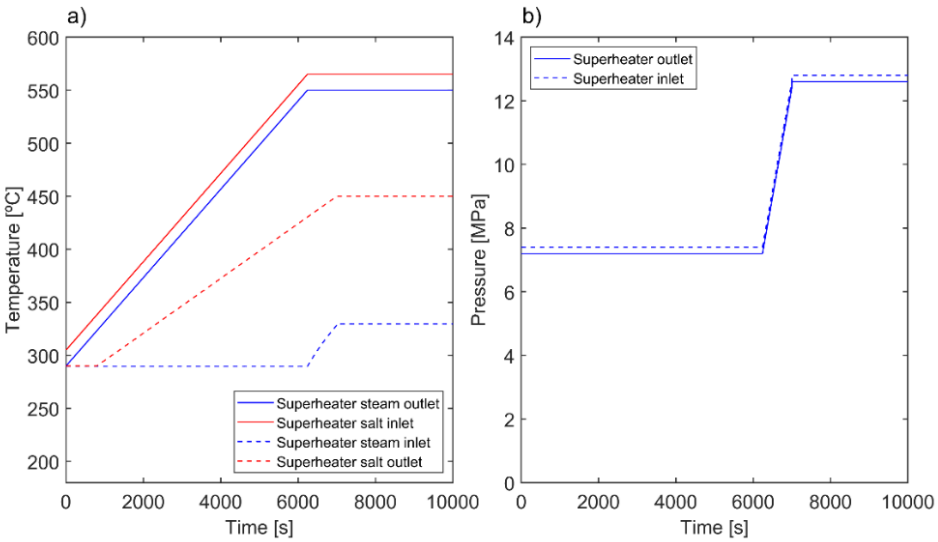

Fig. 4: Temperature and pressure evolution in the superheater during steam generator startup.

3. Methodology

Before performing the creep-fatigue analysis, it is necessary to determine the thermal and pressure stresses occurred during the transient operation of the steam generator. To that end, the methodology presented in (González-Gómez et al., 2017) is used to determine the stress in hot spots of the superheater like header and tube joints as point P shown in Figure 5 in the case of header -type SH. Thermal stress σ^T is obtained according to the European standard EN 12952-3:

$$\sigma^T = \frac{\beta \cdot E}{1-\upsilon} \cdot \left(T_m - T_{r=r_i}\right) \qquad \text{(eq.1)}$$

where β is the thermal expansion coefficient, E is the Young's modulus, υ is the Poisson ratio, T_m is the mean integral material temperature and $T_{r=r_i}$ the inner wall temperature. These two last parameters can be deducted from solving the cylindrical heat diffusion equation restricted only in the radial direction with the initial and boundary conditions shown in eq. 2, using the Crank-Nicholson method (Esfandiari, 2017):

$$\begin{cases} \dfrac{1}{\alpha}\dfrac{\partial T}{\partial t} = \dfrac{1}{r}\dfrac{\partial}{\partial r}\left(r\dfrac{\partial T}{\partial r}\right) \\ T(r,0) = T_0 \\ -k\left.\dfrac{\partial T}{\partial r}\right|_{r=r_i} = h_i \cdot (T_i - T(r_i,t)) \\ -k\left.\dfrac{\partial T}{\partial r}\right|_{r=r_o} = h_o \cdot (T(r_o,t) - T_o) \end{cases} \qquad \text{(eq.2)}$$

The header side heat transfer coefficient h_i, is obtained according to Gnielinski correlation (Serth et al., 2014). On the other hand, the shell side heat transfer coefficient is calculated according to Hilpert correlation (Bergman et al., 2011).

The mechanical stress σ^P is calculated according to EN 12952-3 as well, where P_i is the internal pressure existing in the SH. D_m and e are the average diameter and thickness of the header, respectively:

$$\sigma^P = P_i \cdot \frac{D_m}{2 \cdot e} \qquad \text{(eq.3)}$$

Once both thermal and mechanical stresses are deducted, the total stress appearing at point P is calculated applying two thermal and mechanical stress concentration factors, α_T and α_M, respectively, according to the European standard:

$$\sigma = \alpha_M \cdot \sigma^P + \alpha_T \cdot \sigma^T \qquad \text{(eq.4)}$$

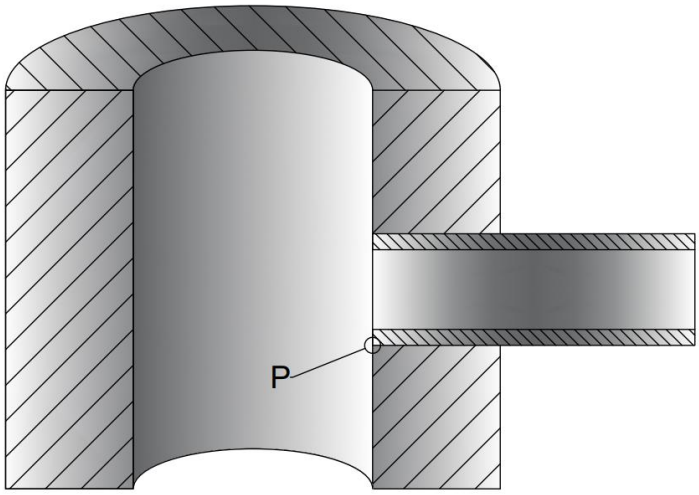

Fig. 5: Tube-header junction

2.1 Creep damage

In first place, the elastic-plastic stress σ is deducted according to the Neuber's equation where ε_{offset} is calculated as shown in (Kalnins, 2016):

$$\sigma^E \cdot \varepsilon^E = \frac{\sigma^2}{E} + \sigma \cdot \left(\frac{\sigma}{K'}\right)^{1/n'} - \sigma \cdot \varepsilon_{offset} \qquad \text{(eq.5)}$$

K' and n' are experimental parameters whose values are summarized in Table 2 which have been obtained by fitting from the experimental data available in (Stoppato et al., 2012), according to the cyclic stress-strain curve, which takes into account the cyclic hardening of the steel.

Tab. 2. Parameters K' and n' for 321H stainless steel according to (Stoppato et al., 2012)**.**

Material	**Temperature (°C)**	**Cyclic stress/strain curve**	
		K' (MPa)	n' (-)
321H stainless steel	540	1928	0.361
	20	2082	0.317

In the Header-type calculation process, the value of elastic-plastic stress should be corrected as mentioned in (Stoppato et al., 2012) multiplying it by a weld strength reduction factor equal to 1.05 according to the ASME Code (ASME, 2004).

Finally, the creep damage is obtained as the summation of the ratios between the duration of the time intervals at which the time is discretized along the lifetime (a total of *N*) and the time to rupture, t_R:

$$D_c = \sum_{i=1}^{N} \frac{\Delta t_i}{t_{R,i}(\sigma_i, T_i)} \qquad \text{(eq.7)}$$

The creep damage is calculated considering 6000 hours per year. The time to rupture is obtained from the European Creep Collaborative Committee datasheets (ECCC, 2005).

2.2 Fatigue Damage

The fatigue damage is calculated according to what it is proposed in (Stoppato et al., 2012). The plastic strain is estimated thanks to the Neuber's rule (eq. 5). Then, the number of cycles N_a to failure is calculated according to the experimental Manson-Coffin curve. In the Header-type analysis, the recommended number of cycles is one half of the N_a obtained due to the welding between tubes and header effect.

Lastly, the fatigue damage is due to the M fatigue cycles during the lifetime and the number of allowable cycles in which these strain ranges result individually, N_a:

$$D_f = \sum_{j=1}^{M} \frac{N_j}{N_{a,j}(\varepsilon_j, T_j)} \qquad \text{(eq.8)}$$

The number of startups considered to estimate the fatigue damage is set to 300 per year.

2.3 Lifetime calculation. Creep-Fatigue interaction

The failure criterion is set by the allowable limit of damage (D_L) according to the ASME Code (ASME, 2004) for the stainless steel 304 and 316 interaction bilinear rule: (1,0), (0.3,0.3) and (0,1). This approximation is taken since there is no available experimental data about creep-fatigue interaction of 321H stainless steel and following the approach used in (Stoppato et al., 2012). The sum of creep and fatigue damages must be lower than the maximum allowable limit of damage D_L as:

$$D_f + D_c \leq D_L \qquad \text{(eq.9)}$$

Lifetime of the superheater is estimated by an iterative process until the total damage set as the sum of creep and fatigue damage converges into the D_L.

4. Discussion of the results

The temporal evolution of the pressure, the thermal and the total stresses during the startup for both designs are depicted in Figure 6. As can be seen, the high thickness of the head for the hairpin-type involves a high thermal inertia and then a larger thermal stress variation is obtained compared to the header-type. The positive thermal stress of the header-type is due to the convective external boundary condition of the hot salt instead of insulated as is the case of the hairpin-type. The steady-state stresses, which are the most important to calculate the creep damage, are around 153 MPa and 170 MPa for the header-type and hairpin-type, respectively.

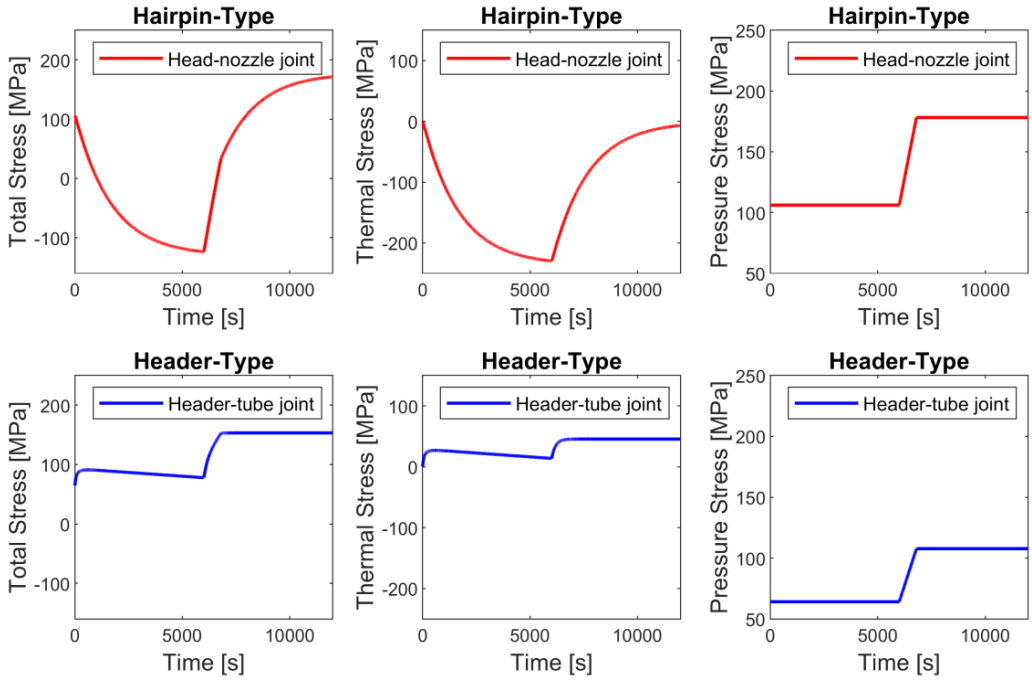

Fig. 6: Stress analysis results.

Figure 7 illustrates the results of the finite element transient thermal analysis at the maximum thermal stress time instant. As can be seen, the temperature difference between the inner and outer wall is around 100 ºC for hairpin-type and around 15ºC for header-type. This great difference is mainly caused by the greater wall thickness of the hairpin-type head over the header thickness. Another important differential factor is the external boundary condition, while the external surface of the header is exposed to the salt flow, the external surface of the hairpin-type head is insulated.

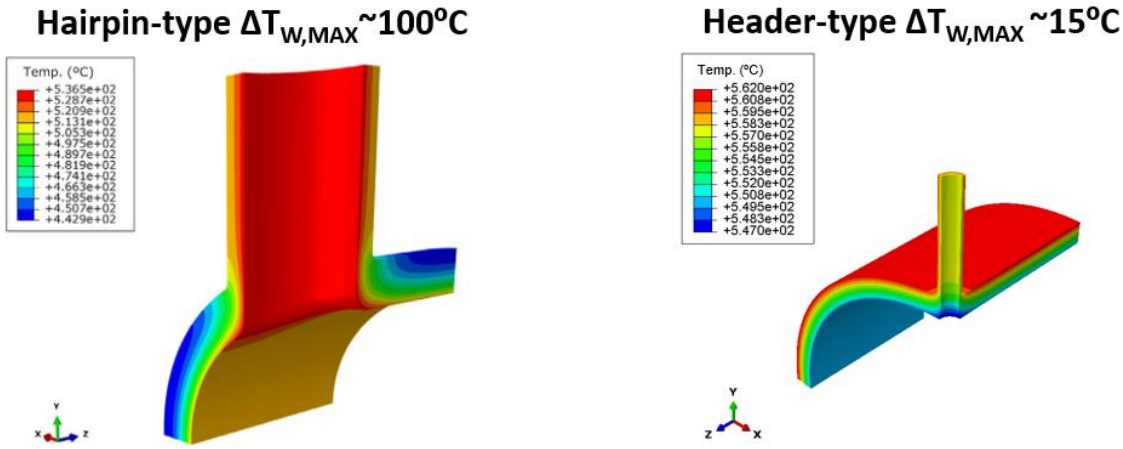

Fig. 7: Finite element transient thermal analysis results.

The creep damage, the fatigue damage, and the lifetime results are depicted in Figure 8. The results show that the creep is the dominant mechanism of damage for the header-type whereas in the hairpin-type both damages have a similar order of magnitude leading to a damage limit value lower than the unity, $D_L < 1$. The results of the lifetime are 15 years and 48 years for the hairpin-type and header-type, respectively. Finally, the comparison study reveals that the header-type presents an important lifetime increase, thus becoming an interesting option to enhance the reliability of the steam generator.

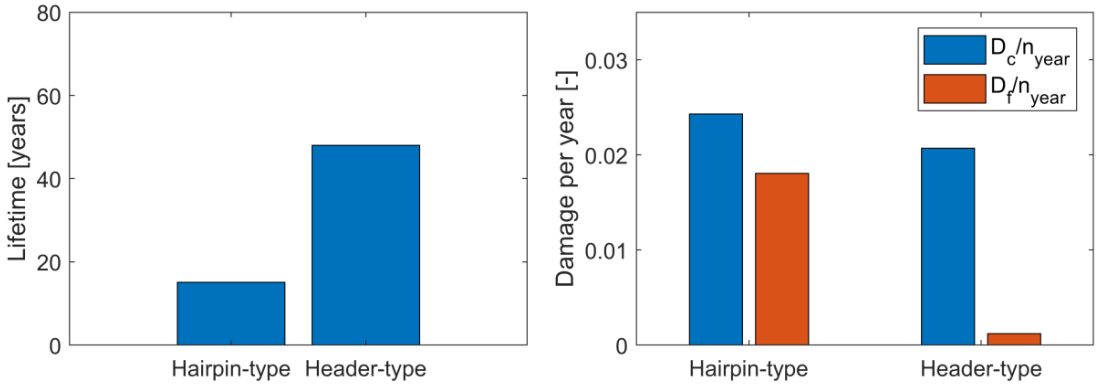

Fig. 8: Lifetime and damage analysis results.

5. Conclusions

The results presented in this document give hints that could illustrate how the header-type design develops an upgraded performance when compared to the hairpin-type, under high temperature and pressure working conditions. Based on the results showed above, the following conclusions are obtained:

- Header-type superheater design reduces 6.6 times the maximum temperature difference between inner and outer walls during a daily start-up.
- The temperature difference reduction is mainly due to the lower metal wall thickness of the header-type design. Consequently, the fatigue damage is practically eliminated in the hot header of the header-type superheater.
- The creep damage appears to be a key factor to estimate the lifetime of the header-type superheater. In contrast, the combination of creep-fatigue damages becomes fatal for hairpin-type superheater obtaining lifetimes much lower than typcial lifetime design targets.
- Header-type superheater shows a lifetime 3 times higher than hairpin-type superheater.
- The good structural results obtained by the header-type superheater suggest that it would be a promising option for solar tower plants operated as “peaker plant”.

6. Acknowledgements

This research is partially funded by the Madrid Government (Comunidad de Madrid) under the project ZEROGASPAIN-CM-UC3M (2020/00033/002) belonging to the program of Multiannual Agreement with UC3M in the line of "Fostering Young Doctors Research" and in the context of the V PRICIT (Regional Programme of Research and Technological Innovation, the Spanish government under the project RTI2018-096664-B-C21 (MICINN/FEDER, UE) and the scholarship “Ayudas para la formación del profesorado universitario” (FPU-02361) awarded by the Spanish Ministerio de Educación, Cultura y Deporte (MECD).

7. References

Aalborg CSP, 2021. Aalborg CSP Concentrated Solar Power steam generators [WWW Document].

ASME, 2004. American Society of Mechanical Engineers. ASME boiler and pressure vessel code, Section III, Division 1, Subsection NH.

Bergman, T.L., Lavine, S.A., Incropera, F.P., Dewitt, D.P., 2011. Fundamentals of Heat and Mass Transfer, 7th ed. John Wiley & Sons, Hoboken.

ECCC, 2005. ECCC data sheets 2005. Etd 47.

Esfandiari, R.S., 2017. Numerical Methods for Engineers and Scientists Using MATLAB, in: Taylor & Francis Group (Ed.), . LLC, Boca Raton, Florida.

Ferruzza, D., Kærn, M.R., Haglind, F., 2019. Design of header and coil steam generators for concentrating solar power applications accounting for low-cycle fatigue requirements. Appl. Energy 236, 793–803. https://doi.org/10.1016/j.apenergy.2018.12.030

González-Gómez, P.A., Gomez-Hernandez, J., Briongos, J.V., Santana, D., 2018. Fatigue analysis of the steam generator of a parabolic trough solar power plant. Energy 155, 565–577. https://doi.org/10.1016/j.energy.2018.04.193

González-Gómez, P.A., Gómez-Hernández, J., Briongos, J.V., Santana, D., 2017. Transient thermo-mechanical analysis of steam generators for solar tower plants. Appl. Energy 212, 1051–1068. https://doi.org/10.1016/j.apenergy.2017.12.128

González-Gómez, P.A., Gómez-Hernández, J., Briongos, J. V., Santana, D., 2019. Lifetime analysis of the steam generator of a solar tower plant. Appl. Therm. Eng. 159, 113805. https://doi.org/10.1016/j.applthermaleng.2019.113805

Kalnins, A., 2016. PVP2008-61397 Twice-yield method for assessment of fatigue caused by fast thermal transient according to 2007 Section VIII-Division 2 1–9.

Mehos, M., Price, H., Cable, R., Kearney, D., Kelly, B., Kolb, G., Morse, F., 2020. Concentrating Solar Power Best Practices Study.

Mehos, M., Turchi, C., Vidal, J., Wagner, M., Ma, Z., Ho, C., Kolb, W., Andraka, C., 2017. Concentrating Solar Power Gen3 Demonstration Roadmap.

NREL, 2009. Solar Advisor Model Reference Manual for CSP Trough Systems.

Serth, R.W., Lestina, T.G., The, S., 2014. Principles , Applications and Rules, Process Heat Transfer (Second Edition).

Stoppato, A., Mirandola, A., Meneghetti, G., Lo Casto, E., 2012. On the operation strategy of steam power plants working at variable load: Technical and economic issues. Energy 37, 228–236. https://doi.org/10.1016/j.energy.2011.11.042

Wagner, W., Kretzschmar, H.-J., 2008. International Steam Tables, 2nd ed. Springer Berlin Heidelberg, Berlin, Heidelberg. https://doi.org/10.1007/978-3-540-74234-0

Appendix: Nomenclature

Abbreviations

ASME	American Society of Mechanical Engineers
CT	Cold Tank
CSP	Concentrated solar power
EV	Evaporator
FW	Feed water
HP	High pressure
HT	Hot tank
LP	Low pressure
PH	Preheater
R	Receiver
RH	Reheater
SGS	Steam Generator System
SH	Superheater

Symbols

D_m	mean diameter (m)
D_c	creep damage
D_f	fatigue damage
D_L	damage limit
E	Young modulus (MPa)
e	thickness (m)
H	hours of operation (hours), dwell time period (hours)
h	heat transfer coefficient (W/m^2K)
K'	strain hardening parameter (MPa)
K	thermal conductivity (W/mK)
N_a	number of allowable cycles
n'	strain hardening exponent
P_i	internal pressure (Pa)
r	radial direction (m)
r_e	outer radius (m)
r_i	inner radius (m)
T	Temperature (ºC)
t	time (s)
t_R	time to rupture (hours)

Greek Symbols

α	stress concentration factor, thermal diffusivity (m^2/s)
β	thermal expansion coefficient (K^{-1})
ν	Poisson's ratio
σ	stress (MPa)
ε	strain
ε_{offset}	strain offset